Numerical Study on Thermal Separation Performance in Vortex Tube Using Different Working Tubes

Fawad Ali*, Muhammad Ali Kamran, Mehran Meer***, Muhammad Hamza Awan**, Ameer Hamza**, Muhammad Alam Zaib Khan****

*Faculty of Sciences, Aix-Marseille University, Jardin du Pharo, 58 Boulevard Charles Livon, Marseille, 13007, France
**Department of Mechanical Engineering, University of Engineering and Technology Peshawar, 25120, Pakistan
***Tecnical Faculty, Friedrich-Alexander-Universität Erlangen-Nürnberg, Erwin-Rommel-Straße 60, Erlangen, 91058, Germany

Abstract- Cooling driven through halogenated gases is putting our environment at risk as its leakage contributes to global warming. One of the green alternative technologies to the current vapor compression technology is cooling through vortex tube, a thermal separation phenomenon. It is a simple device in which pressurized gas is tangentially passed to create two swirls, one with high temperature and the other with the cold temperature that can be used for cooling applications. This device has no moving parts and requires low maintenance. This paper aims to investigate the effect of different working tube designs on the performance of vortex tube using a numerical approach. These designs include 1° converging, 1° diverging and a straight tube associated with 16° bend shape. For this purpose, a test rig was fabricated to validate the standard model of vortex tube experimentally. It was found that cold stream temperature dropped as the inlet pressure increased and reached 273 K at 5 bars. Further investigations were performed via computational fluid dynamics approach using compressible air flow model in Fluent code. Based on results, 1° diverging bend tube shows the highest performance and overall COP has been increased by 40 % of the standard model.

Index Terms- Computational Fluid Dynamics, Vortex Tube, Bend Angle, Thermal Separation, Cold Mass Fraction

I. INTRODUCTION

A vortex tube is a device that splits a pressurized gas flowing through it into two streams; one in the core region and the other in the peripheral region such that compared to the inlet, temperature in the core region is low while temperature of the peripheral stream is high. Thus, it converts pressure energy into thermal energy in the form of temperature difference. The cold stream can be utilized for refrigeration purpose, providing a mean to reduce the use of environmentally hazardous fluorinated refrigerants [1], which have been estimated to contribute 15-20% to the overall global warming trend [2]. Unlike traditional refrigeration systems, vortex tube uses air as a refrigerant. It has a compact size and does not require maintenance due to its simplistic design. The vortex tube is more attractive in small-scale cooling due to its simple design and compactness compared to the widely used vapor compression system. They have found usage in cabin cooling, electric panels cooling, spot cooling, process cooling, and personal air suits [3]. Moreover, vortex tube cooling has also been introduced to light vehicle air conditioning systems to avoid the leakage of hazardous refrigerants in any car accidents [4,5,14].

Primarily, a vortex tube consists of an inlet, vortex chamber, working tube, and a frustum valve as shown in Fig. 1. Compressed air enters the vortex chamber tangentially, inducing swirls in the flow. The swirls gain strength while flowing through the working tube, splitting the flow into two sets of vortices possessing considerable difference in temperature and velocity. The core vortex has low velocity and temperature whereas the outer vortex exhibits higher velocity and temperature. In the uniflow arrangement, both the vortices flow in the same direction. However, if an obstruction is placed in front of the core vortex, the fluid rebounds, and cold fluid comes out of the vortex tube from the other end. This type of arrangement is known as counter vortex tube, and is more common due to its better performance.

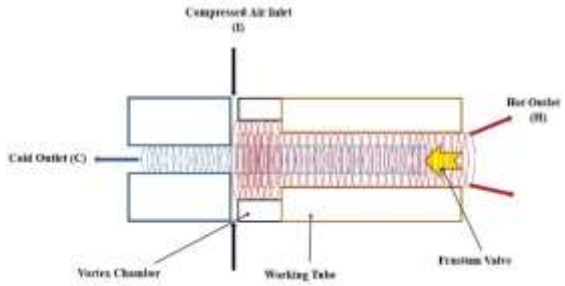

Figure 1 Vortex tube schematic diagram

The design of vortex tube was first presented by a French Metallurgist and Physicist, George Joseph Ranque [6] in 1933, who proposed that energy separation occurs due to expansion in the core vortex and compression in the peripheral vortex. Due to a lack of interest by the researchers, this idea was overlooked for many years until a German physicist Hilsch [7] in 1947, conducted several experiments and attributed the energy separation phenomena to adiabatic expansion and compression processes as well as friction in internal layers. The energy separation phenomenon is thus termed Ranque-Hilsch effect. Despite its simplistic design, understanding the energy separation has remained a perplexing problem in the area of heat transfer. Different theories have been proposed to explain the Ranque-Hilsch effect. Kassner and Knoernschild [8] studied the velocity and shear stress distribution in the radial direction which showed that free and forced vortices were the driving agents for energy separation phenomena. Fulton [9] also supported this theory by studying the angular velocities at the core and peripheral region of the vortex tube. Kurosaka [10] introduced the acoustic streaming theory. On varying the sound intensity level from 75 dB to 120 dB, a temperature difference of 10°C was noted. He argued that the swirl flow effectuates sound waves which trigger temperature shift along the radial direction in the vortex tube. Stephane et al. [11] proposed that Görtler vortices were responsible for energy separation phenomena. Ahlborn and Groves [12] reported secondary flow within a vortex tube. They reported that the cold mass flow coming out of the cold end of the vortex tube is much lower than the return flow from the frustum valve. They argued that a secondary circulation imbedded into the primary vortex moves the fluid from the core stream back to the outer regions. A few computational fluid dynamics (CFD) studies have also been conducted to understand the flow behavior within a vortex tube. Frohlingsdorf and Unger [13] modeled a 2D axisymmetric tube, and concluded that the difference in angular velocities of the two layers caused by internal friction is responsible for inducing the temperature difference. Bej and Sinhamahapatra [23] conducted a CFD study of vortex tubes connected in series, and observed that tangential shear drives the energy from cold fluid zone to hot fluid. The study by Kazantseva et al. [15] supported the secondary flow theory. Sohn et al. [17] used surface tracking method to visualize the flow trajectories in a counter flow vortex tube. Sudden changes in the vortex tube trajectory indicating stagnation points were observed at the tube wall at all inlet pressures. The stagnation points were also observed in the computational investigation reported in the paper.

Some CFD studies have been devoted to identifying the 'best' turbulence model capable of predicting the vortex tube flow. Although, most of the popular available models were able to predict the flow features satisfactorily, disagreement exists in the available literature on the selection of turbulence model for studying the vortex tube problem. Kazantseva et al. [15] on investigating SST k-ω and k-ε turbulence models noted that both exhibited the same ability to model the precession vortices. Skye et al. [16] also investigated the effect of difference turbulent models in predicting the vortex tube flow using 2D axisymmetric model. Comparison with experimental results showed the standard k-ε model to be the most accurate followed by the RNG k-ε model while the Reynolds Stress Model (RSM) was not able to reproduce the experimental findings satisfactorily. Eiamsa-ard and Promvonge [18], in addition to turbulence models compared the effect of different computational schemes (hybrid, second-order, Upwind, QUICK) using the staggered finite volume approach. Marginal difference in results was noted with a change in the computational scheme while algebraic stress model (ASM) showed better agreement with the experimental data compared to the standard k–ε model., Rattanongphisat et al. [19] claimed good agreement of the k-ε turbulence model with experimental data. Baghdad et al. [21] in an effort to identify the best turbulence model for the vortex tube problem investigated four turbulence models namely, the k–ε, k–ω and SST k–ω two-equations model and the second moment closure model (RSM). Although all the models predicted the flow features fairly well, the RSM model showed better agreement of hot and cold temperatures with the experiments while a comparison of Spalart-Allmaras and RSM model with experimental study reported by Thakare and Parekh [22] showed RSM to underpredict the performance. Radomir et al. [27] after their study and Nikitin et al. [25] based on a literature review of some recent CFD studies have recommended the k-ε model, while Niknam et al. [24] found the three equation turbulence model (k-kl- ω) to be in agreement with experimental data compared to other models. Guo and Zhang [26] investigated the vortex breakdown phenomena in a vortex tube and studied the effect of varying cold mass fraction on the vortex structures. A limited range of cold mass fraction was identified which results in formation of bigger vortex cores, and hence better energy separation. Radomir et al. [27] performed CFD simulation in STAR-CCM+ codes

to investigate turbulence modeling and Xiangji [28] critically reviewed CFD techniques and visualization methods in order to provide a guideway for future exploration of RHVT studies. Several LES studies have also been conducted to explain the vortex breakdown phenomenon. Farouk [20] studied this phenomenon using an unsteady 2D axisymmetric model with CFD-ACE+ codes for the gas mixture. The study investigated streamlines flow patterns using the Large Eddy Simulation turbulence model which predicted secondary circulation in RHVT. The simulations indicated the axial and azimuthal velocities to be the dominant components. In the inner core, very negligible azimuthal velocity was predicted which is contrary to the general perception that in counter flow Ranque–Hilsch vortex tube, the entire core flow is a forced vortex. The small peripheral region was predicted to have free vortex like characteristics. The radial velocity which had the smallest magnitude was found to be directed towards the tube center through most of the tube volume and towards the tube near the wall. The instantaneous streamlines showed the presence of small vortices throughout the vortex tube. However, the small vortical structures were found to be more prominent in the inner core regime. Alekhin et al. [25] examined different turbulence models for 3D double circuit vortex tube using CFX codes. The obtained results for LES model were more accurate, predicting the high radial velocity and sudden change in total pressure are the sources of energy separation.

Recent advancements have enabled the CFD technique to be used as a design tool for RHVT to avoid material and machining costs. Different parametric studies were conducted for optimization of vortex tube using CFD tool. In this scenario, Aljuwayhel et al. [29] varied the length of the hot tube (10 cm to 30 cm) with achieving 2.6% temperature drop and varied tube diameter (1.5 cm to 2 cm) with 4.4%, 2 cm to 3 cm with 24% temperature drop respectively. Behra et al. [30] and Bramo [31] investigated the effect of cold orifice diameter, the number of nozzles, Length to diameter ratio, and mass fraction on the performance of vortex tube. Pourmahmoud et al. [32] proposed nozzle design optimization by studying different nozzle heights and lengths respectively. Thakare [22] examined the effect of the different gas media among which nitrogen has best and CO_2 has poor performance. Rafiee et al. [33] optimized the hot side of RHVT using different bend angles. It was found that 16 degrees angle of curvature shows the best performance. Kandil and Abdelghany [34] carried out a CFD analysis to study the effect of the adiabatic wall, conduction wall and fins wall on the performance of RHVT. Bazgir et al. [35] performed CFD simulations to analyze the effect of straight, convergent, and divergent hot tube on the performance of RHVT. Shamsoddin [36] studied the effect of the number of nozzles and proposed a circular chamber as a vortex generator to reduce the number of nozzles.

Based on the above discussion, it is inferred that the vortex tube has two types of parameters i.e., operating parameters and geometrical parameters. The current issue that exists with the operating parameter is it needs high pressure to attain thermal separation. That's why it makes the vortex tube less attractive to use for cooling applications as it requires an average of 5 bars of pressure which is available from a medium-size compressor. One approach, that can be helpful to resolve this issue is to explore further studies of geometrical parameters affecting thermal separation. In another word, the coefficient of performance of vortex tube is very low as compared to the conventional refrigeration system. Therefore, the current study is dedicated to making an alteration to geometrical parameters so to increase the coefficient of performance of vortex tube. This article describes the effect of different working tubes of vortex tube such as bend tube, 1° diverging, and converging tube on the coefficient of performance of vortex tube.

II. Physical Setup

The effect of different working tubes designed on the performance of vortex tube is studied through a numerical approach. However, for validation of numerical results, a physical setup is made to test the experimental results of the vortex tube as shown in Figure 2. A standard model vortex tube is manufactured for the test rig. Aluminum is chosen as a design material for its better machinability, lightweight, and low cost comparatively. The geometrical specification of this model is given in Table 1.

Table 1 Geometrical Specifications of Standard Model Vortex Tube

Measurement	Value	Unit
Total Inlet Area	18.84	mm^2
Nozzle Height	1.57	mm
Nozzle Width	2	mm
Working Tube Length	150	mm
Cold Exit Diameter	5	mm
Hot Exit Diameter	12	mm
Working Tube I. D	14	mm

The setup consists of an inlet pipe acting as a source of compressed air to the vortex tube. To account for variable flow, a control valve has been installed at the inlet pipe. To measure the flow rate, rotameters are installed at the inlet and cold outlet, and hot outlet so that cold mass fraction can also be measured. A cold mass fraction (α) is the ratio of mass flow rate at a cold outlet to the total mass flow rate inlet. The flow diagram is shown in Figure 2, where the compressed air flows through the inlet of

the vortex tube to separate into two outlets. For the pressurized air source, a two-stage air compressor is introduced at the main inlet of the test rig and the airflow is initiated. The inlet valve is gradually opened and fixed at 5 bars pressure indicated by the pressure gauge. Since the vortex tube is a thermal device, therefore its output will be measured in temperature quantity. For this purpose, T-type thermocouples are chosen for their better accuracy at low range temperatures. These thermocouples are fixed at the inlet as T_1, hot outlet T_2, and cold outlet T_3 as shown in the sketch diagram.

(a)

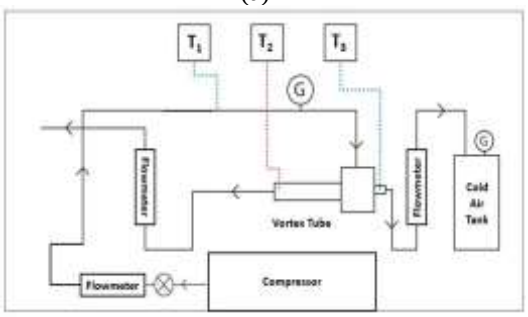

(b)

Figure 2 (a) Experimental setup of vortex tube test rig (b) Flow diagram of experiment

Based on experimental results, it is found that as the inlet pressure increases, the cold outlet temperature also drops. On the other hand, when the frustum valve is released at the hot side, the temperature also gets elevated at both sides. This shows that the cold mass fraction has also a significant effect on temperature separation in a vortex tube. From the experimental results, the lower cold mass fraction yields a high drop in cold temperature. However, it is still difficult to decide whether lower cold mass fraction improves or worsen the thermal separation performance in a vortex tube. This will be discussed in the later section by looking at the Coefficient of Performance (COP) analysis. Since it is more costly and time-consuming to manufacture different featured vortex tubes such as 16° bend vortex tube, 1° diverging, and converging tubes associated with bend vortex tube. Therefore, the experimental results of the standard model will be compared with CFD results which will create a baseline for numerical approach, and later the rest of the models will be studied using CFD analysis.

III. Numerical Model

Just like the experimental model, a similar geometry of vortex tube is replicated for the CFD model in CAD software (Solidworks). A structured mesh strategy has been adopted to generate a computational domain. The reason for using structure meshing is due to the existence of steep pressure gradient across the swirl flow domain. The model is imported in ICEM-CFD where hexahedral cells are generated by keeping high orthogonal quality. The blocks are split via the O-grid methodology. Different cross-sections of the meshing domain have been shown in Figure 3. The geometrical domains for operating conditions are also specified using the surface selection method as inlet, outlets, and wall which will be considered as boundary conditions in CFD solver. A similar methodology has been adopted to generate three other models of vortex tube i.e., 16° bend vortex tube, 1° diverging working tube, and 1° converging vortex tube associated with bend vortex tube.

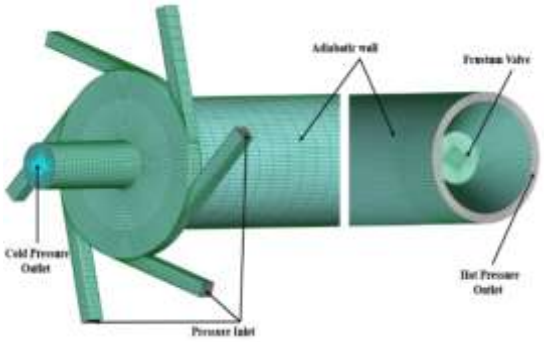

(a)

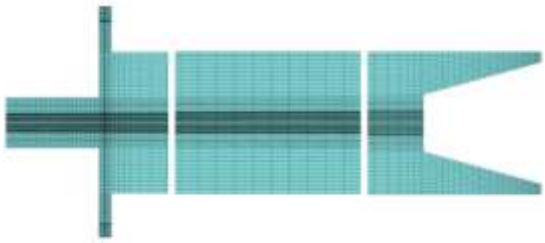

(b)

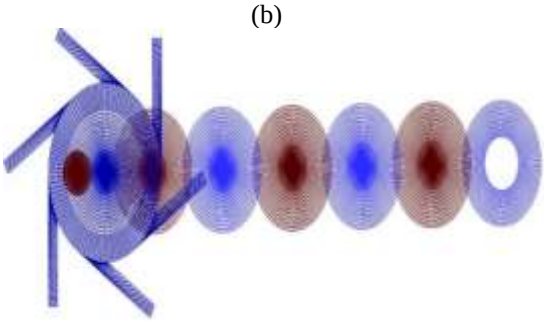

(c)

Figure 3 Computational domain of vortex tube of (a) Three Dimensional VT (b) YZ plan cross-section (c) XY plan cross-sections equally spaced slices

A. Boundary Conditions

To initialize the approximate solution, it is necessary to specify the solver boundary conditions, and

medium of the computational domain. In this study, Fluent code will be used as a solver which can work only on unstructured mesh. For this purpose, the mesh was converted into an unstructured form in ICEM-CFD. Now the mesh is ready for further steps to define and quantify the boundary conditions based on the experimental values.

Inlet: at the inlet, the pressure inlet boundary conditions were defined and gauge pressure values in pascals were specified. For validation, 500000 Pa pressure as gauge pressure and thermal boundary conditions as 305 K inlet temperature were defined.

Outlets: Since there are two outlets, therefore, two outlet boundaries (Hot & Cold) were defined as,

I. Hot Pressure Outlet: at the hot side, pressure outlet boundary conditions were defined. The value of pressure is varied from 1 bar and onward. This is because a hot pressure outlet is a driving agent to vary the cold mass fraction on cold outlet.

II. Cold Pressure Outlet: at the cold side, pressure outlet boundary conditions were defined. The pressure values are kept at ambient conditions.

Walls: The walls are defined with stationary and adiabatic wall boundary conditions.

It is necessary to define a proper simulation setting while using Fluent Solver. Therefore steady-state simulations with pressure-based solver selection were carried out. The following conservation equations were defined inside Fluent Solver:

Continuity Equation:

$$\frac{\partial}{\partial x_i}(\rho u_i) = 0 \tag{1}$$

Momentum Equation:

$$\frac{\partial}{\partial x_j}(\rho u_i u_j) = \frac{\partial p}{\partial x_i} + \frac{\partial}{\partial x_j}\left[\mu\left(\frac{\partial u_i}{\partial x_j} + \frac{\partial u_j}{\partial x_i} - \frac{2}{3}\delta_{ij}\frac{\partial u_k}{\partial x_k}\right)\right] + \frac{\partial}{\partial x_j}\left(\overline{-\rho u_i' u_j'}\right) \tag{2}$$

Energy Equation:

$$\frac{\partial}{\partial x_i}\left[u_i \rho\left(h + \frac{1}{2}u_j u_j\right)\right] = \frac{\partial}{\partial x_j}\left[K_{eff}\frac{\partial T}{\partial x_j} + u_i\left(\tau_{ij}\right)_{eff}\right] \tag{3}$$

where,

$$K_{eff} = K + \frac{C_p \mu_t}{Pr_t} \tag{4}$$

The first term on the left side of the Eqn. (3) represents the rate of total energy lost due to convection by fluid element whereas the two terms on the right-hand side represent heat transfer due to conduction and viscous dissipation, respectively.

Ideal Gas Equation:

To account for fluid compressibility flow behavior, the ideal gas equation is employed given below:

$$p = \rho R T \tag{5}$$

Standard K-ε model:

To capture turbulences in the flow domain, the two equations turbulence model, Standard K-ε model is employed to close the RANS equations. The transport equations for turbulence kinetic energy and dissipation rate are solved by using Fluent. These are:

$$\frac{\partial}{\partial t}(\rho k) + \frac{\partial}{\partial x_i}(\rho k u_i) = \frac{\partial}{\partial x_j}\left[\left(\mu + \frac{\mu_t}{\sigma_k}\right)\frac{\partial k}{\partial x_j}\right] + G_k + G_b - \rho\varepsilon - Y_M \tag{6}$$

$$\frac{\partial}{\partial t}(\rho \varepsilon) + \frac{\partial}{\partial x_i}(\rho \varepsilon u_i) = \frac{\partial}{\partial x_j}\left[\left(\mu + \frac{\mu_t}{\sigma_\varepsilon}\right)\frac{\partial \varepsilon}{\partial x_j}\right] + C_{1\varepsilon}\frac{\varepsilon}{k}(G_k + C_{3\varepsilon}G_b) - C_{2\varepsilon}\rho\frac{\varepsilon^2}{k} \tag{7}$$

$$\mu_t = \rho C_\mu \frac{K^2}{\varepsilon} \tag{8}$$

In the above equations, μ_t represents the turbulent viscosity, G_k is the turbulent kinetic energy generation due to mean velocity gradient, G_b represents the turbulent kinetic generation due to buoyancy and Y_M is the contribution of the fluctuating dilatation incompressible turbulence to the overall dissipation rate respectively. Where the constants $C_{1\varepsilon}$, $C_{2\varepsilon}$, and $C_{3\varepsilon}$ are having 1.44, 1.92, and 0.09 values, respectively. Similarly, the turbulence Prandtl numbers for the k and ε are $\sigma_k = 1.0$ and $\sigma_\varepsilon = 1.3$. Finally, Eqn. (8) provides the mathematical mean to find out the eddy viscosity for the K-ε model.

A SIMPLE algorithm is selected for velocity pressure coupling whereas for the discretization of convective terms second-order upwind schemes are used. The convergence criteria on the residual scale are set to 10^{-6} for energy and 10^{-3} for both continuity and momentum. For turbulence modeling, the standard k- ε model is considered for the overall simulations as it has a wide range of fluid flow applications. The Y+ value is kept between 30 to 300 since most of the simulations are carried out using standard wall functions.

B. Grid Independence Study

The grid sensitivity analysis is necessary for any CFD simulation fluid flow problem. It shows how the mesh size affects the accuracy of the solution. Once proper mesh size is identified i.e., the number of cells, then any relationship or parametric study of flow variables can be conducted from CFD results. Another advantage of grid independence study is to reduce the computational and time costs.

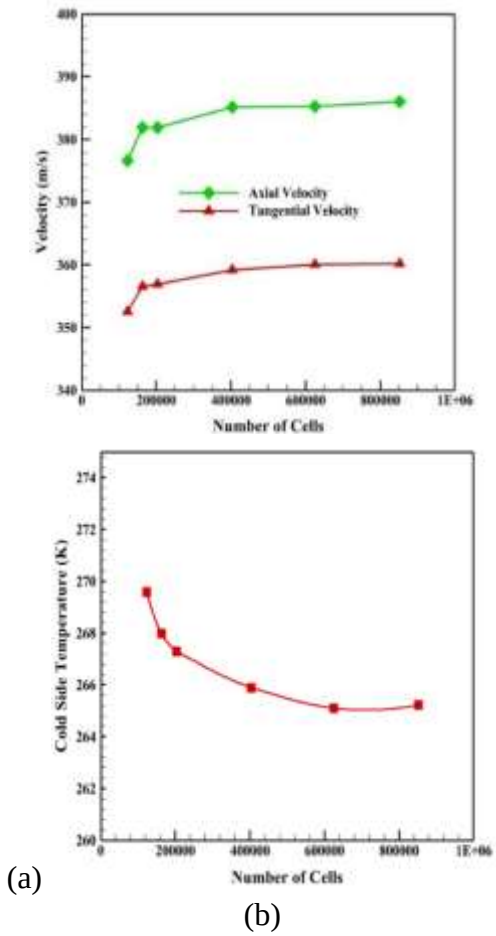

Figure 4 Grid independence study (a) Axial and tangential velocities curves using different number of cells (b) Cold temperature vs number of cells

Referring to Figure 4, it is observed that the value of maximum axial velocity is 376.6 m/s when the total number of cells is 0.12 million. However, when the cells are increased in the meshing domain, the axial velocity is also varied up to a certain limit of 385 m/s. Based on the mesh reports by exceeding 4 lack cells, the solution is almost converged to a certain value of axial velocity and thus it can be concluded that the model of 0.4 million cells will give an optimized value that avoids solution time consumption and computational costs.

A similar analysis is carried out for tangential velocities using different mesh models. Based on the results, the tangential velocity is 352 m/s for the number of 0.12 million cells is obtained. However, the value is further converged to 360 m/s when the number of cells is exceeded above 4 lack cells.

Since the temperature separation of the vortex tube is the focus of this discussion, the temperature sensitivity for a different number of cells should also be analyzed. From Fig. 4 (b), the cold temperature reached approximately 270 K for low number cells. However, as the number of cells increased above 4 lack cells, the temperature values are converged to 265 K. Based on this discussion, it is concluded that for current simulations, the mesh size should be of 4 lack cells or above, to get grid independent CFD result.

IV. Results and Discussions

It is necessary to validate the numerical and experimental results to proceed with further investigations using the numerical approach confidently. The experimental results are compared with numerical results in terms of cold mass fraction (α) and cold temperature. The reason for selecting cold temperature is because the cold mass fraction and cold temperature are the main parameters for calculating the coefficient of performance of vortex tube. From both experimental and numerical results, it is seen that cold side temperature is increasing as the cold mass fraction approaches unity (shown in Figure 5).

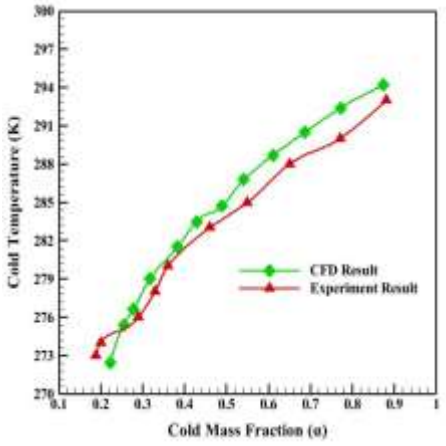

Figure 5 Comparison of Experimental and CFD results of vortex tube for validation

By looking at the plot, it can be observed that both results almost match when the cold mass fraction increased from 0.25 to 0.5. Interestingly, this range is needed for further calculations of finding coefficient of performance. This indicates that most of the results will eventually yield a minimum numerical error. On the other hand, the maximum percentage error based on the above results is 0.8%. This maximum error observed at 0.78 cold mass fraction is due to the application of high gauge pressure on the hot side of the vortex tube. This issue can be avoided by modeling a wider frustum valve instead of using a hot outlet pressure driving mechanism in CFD. From this discussion, it is inferred that the current CFD results are in good agreement with the physical experimentation.

A. Design of Different Working Tubes

As already mentioned, different working tubes are generated in ICEM-CFD to study the effect of the designed working tube on the coefficient of performance of the vortex tube. Figure 6 shows the current models which are used to be considered for analysis. For comparison, the standard model vortex

tube, the 16° bend vortex tube, 1° diverging and 1° converging vortex tube associated with 16° bend angle are considered.

The models associated with 16° bend are the modified form of the standard model vortex tube. The geometrical specifications are also identical in terms of inlet area and the number of nozzles. For simplicity, these models are named straight vortex tube (straight VT), bend vortex tube (bend VT), diverging vortex tube (diverging VT), and converging vortex tube (converging VT). To clarify the bend angle, it is defined between two plans such that each plan is normal to the outlet. This can be achieved by drawing a circle having a radius defined at an angle of 16° and an arc equal to the length of the vortex tube. Similarly, the angle of divergence is also defined based on trigonometry. For this purpose, an extra radial length is calculated for hot outlet circular geometry based on the 1 degree and 150 mm working tube length of the vortex tube. In the same way, the angle of convergent is also calculated for converging VT.

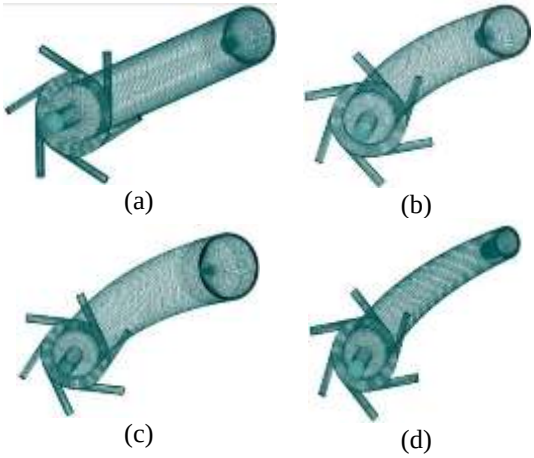

Figure 6 Computational domain: (a) Straight VT (b) Bend VT (c) Diverging VT (d) Converging VT

For analysis, each model is simulated, and different flow fields are investigated. The time taken by simulations is very low as compared to investigation with an experimental approach. Similarly, CFD tools also provide a facility to explore and measure any flow variable at any point inside the computational domain. For this reason, the current numerical investigations are mainly focused on the flow pattern of the mentioned models. This includes the velocity flow field, pressure distribution, and behavior of turbulent viscosity. This will identify the major causes of improvement in the thermal separation of featured geometry vortex tubes.

B. Effect of Bend Angle on Thermal Separation

Previous studies have shown that bending the working tube of the vortex tube can improve the performance of the vortex tube. From the literature, it has been found that the optimized angle of bend for vortex tube is 16 degrees [33]. For this reason, the bend angle for current study has been selected as 16°.

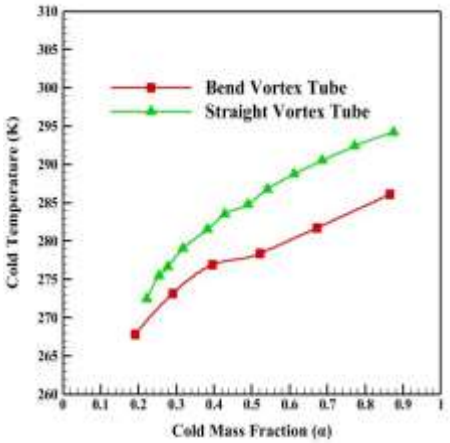

Figure 7 Comparison of the cold temperature of Straight VT and Bend VT at different cold mass fraction

The performance of the bend vortex tube is compared with the standard model vortex tube. For this purpose, the cold temperature is monitored at varying cold mass fractions. Figure 7 shows that cold temperature increases with an increase in cold mass fraction at 5 bars constant pressure for both vortex tubes. However, both models experiencing thermal separation in different manners. It is observed that cold temperature increases rapidly with cold mass fraction in straight VT however in bend VT the cold temperature increases slowly with an increase in cold mass fraction. Since for cooling applications, the desired flow rate is ranging from 40% to 60 %, therefore it is found that for this range of cold mass fraction, the cold temperature of bend VT lies between 277 K and 280 K. However, for a similar range of cold mass fraction, the cold temperature of straight VT lies between 282 K and 288.5 K. This makes the bend VT desirable for cooling since the overall cooling temperature curve bend VT lies below than that of straight VT.

These findings also verified the previous results of performance improvement by using bend vortex tube. This idea can be further extended to generate new models either based on changing the axial length or radial length. The previous studies have shown an appreciable improvement in the performance of vortex tube by a varying angles of cone [35]. Therefore, further explorations to bend the vortex tube is done by generating a 1°degree cone angle to the existing model. An inward cone angle yielded a converging tube whereas an outward cone angle yielded diverging tube.

C. Comparing Diverging and Converging Vortex Tubes

By using a similar methodology, CFD simulations are carried out for converging VT and diverging VT. Figure 8 shows the results of cold temperature distribution obtained at varying pressure and cold

mass fraction for both converging VT and diverging VT.

It is observed that by decreasing the inlet pressure in both converging and diverging VT, the cold side temperature increases and vice versa. At 4 bars pressure the cold temperatures are monitored for converging and diverging VT. It is found that the cold temperature of diverging VT is lowered from converging VT by almost 6 degrees at 60% cold mass fraction. similarly, at 5 bars pressure, the cold temperature of diverging VT is lower than converging VT. From the results, it is found that cold temperature for diverging VT is 274 K whereas that of converging is 279 K at 40% cold mass fraction. A similar trend can also be seen for 6 bars pressure where the cold temperature of diverging VT is lowered than converging VT by 6 degrees when the cold mas flow rate is the same as hot mass flow rate.

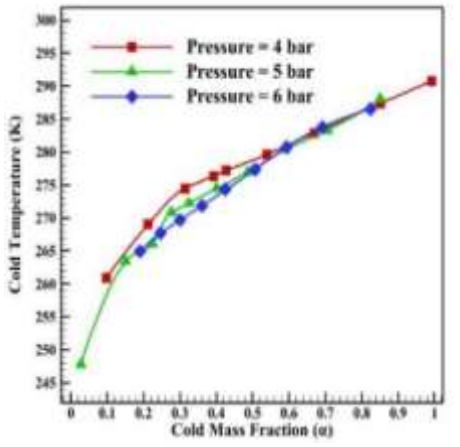

(a)

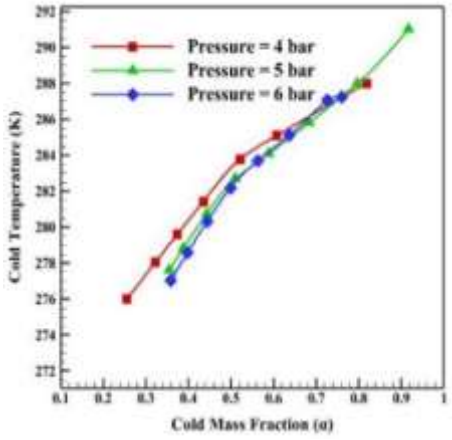

(b)

Figure 8 Cold temperature curves at different pressure conditions: (a) Diverging VT (b) Converging VT

Similarly, the temperature curves also explain the variation of cold temperature slope at different cold mass fraction values. Rapid variations in cold temperature are seen in diverging VT when the cold mass fraction is in the range of 10% to 30%, however, the variations are slowing down as the cold mass fraction exceeds 30%. This effect makes diverging VT attractive for cooling applications as the desirable range of cold mass fraction lies between 40% to 60% where its temperature variation is loosely affects. On the other hand, the fast variations in the cold temperature of converging VT occur between 10% to 52% cold mass fraction. Due to this phenomenon, the overall performance of converging VT is degraded. It will be quantified in the later section using a coefficient of performance analysis.

Next, to look at some causes behind the difference in thermal separation of converging VT and diverging VT a new parameter ξ is defined as below,

$$\xi = \frac{z}{L} \quad (9)$$

It is the ratio specified length "z" to the total length "L" of the working tube. With the help of "ξ" at any point, data can be accessed in the flow domain provided that radial length is variable.

By looking at Figure 9, the temperature distribution along the radius of the vortex tube for both cases have been calculated. It can be inferred that for the convergent tube, the temperature curves show narrow symmetry while for diverging tube, the temperature curves show broad symmetry along the radial length. This is because in the convergent tube the provided radius is smaller which limits the circular flow. However, the defined boundary conditions are also to be satisfied that is, adiabatic wall condition therefore a sudden variation in the temperature curve can be seen. On the contrary, the diverging tube has diffused area and therefore the variation in the temperature curve is lower.

Considering ξ = 0, the minimum and maximum temperatures found in diverging VT are approximately 274 K and 308 K whereas in converging VT these temperatures are 279 K and 307 K respectively. In other words, the thermal separation in terms of temperature difference for converging VT and diverging VT is 28 K and 34 K respectively. On the other hand, by considering ξ = 0.2, the minimum and maximum temperatures for converging VT and diverging VT are 290 K, 317 K, and 290 K, 315 K respectively. This means that thermal separation, in this case, is reversed for these models since converging VT has 27 K and diverging VT 25 K temperature differences respectively. It shows that converging VT has good thermal separation performance at z = 30 mm where extraction of cold flow is impossible. On the other hand, the diverging VT has good performance at z = 0 mm which is the cold orifice region, and therefore based on temperature analysis diverging VT shows better performance.

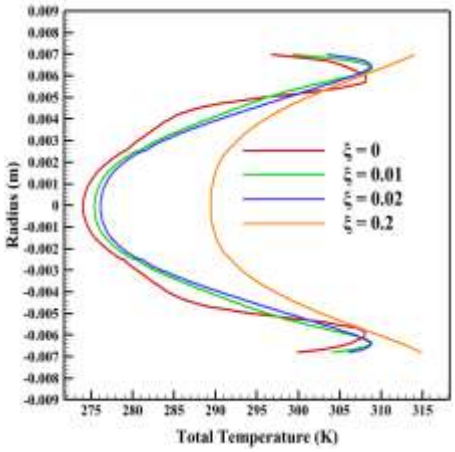

(a)

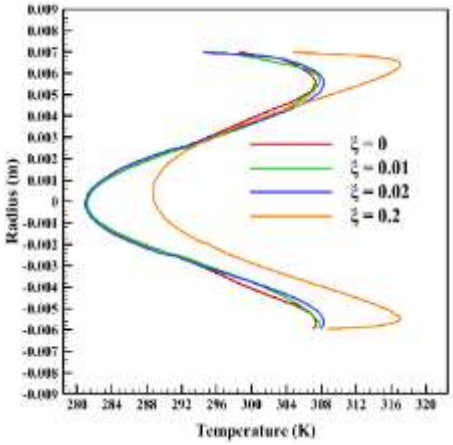

(b)

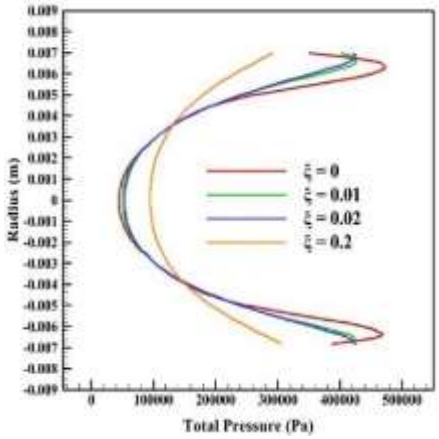

(c)

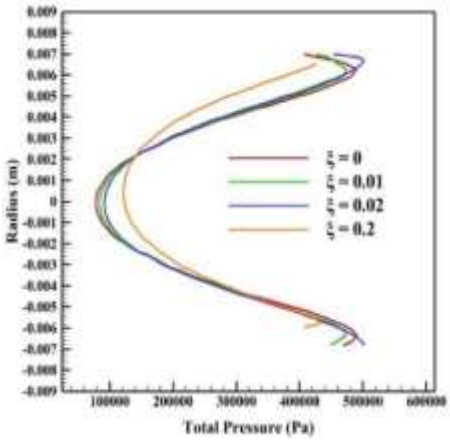

(d)

Figure 9 Temperature distribution along radial length: (a) Diverging VT (b) Converging VT, Pressure distribution along the radial length for (c) Diverging VT (d) Converging VT

Similarly, the total pressure distribution for converging and diverging vortex tube has been shown. By looking at the expansion of compressed air, it is clearly found that the pressure is very low around central axis as compared to peripheral region. In the case of converging VT, the pressure is expanded to 80 KPa as its lowest pressure whereas in diverging VT the minimum pressure drop is 50 KPa. The reason for 30K Pa extra pressure in converging VT is the converging geometry which does not allow pressure to drop further whereas in diverging VT geometry there is extra space on the hot side as a result pressure attains very minimum value during expansion.

Another performance indicator is to check pressure distribution at different values of ξ. For ξ = 0.2, the minimum and maximum pressure obtained is approximately 100 KPa and 300 KPa in diverging VT whereas in converging VT these values are 120 KPa and 430 KPa respectively. These values indicate that pressure expansion at z = 30 mm away from the nozzle is distributed such that for converging VT there is still high pressure exists as compared to diverging VT. It can be concluded that diverging VT utilizes the pressure drop more than converging VT. Since by definition a vortex tube convert pressure energy to thermal energy, therefore, it is the reason that divergent VT yields better performance than convergent.

Finally, an assessment is made to evaluate the performance of these two vortex tubes models by comparing them with the previous bend VT. These models are compared using cold temperature profiles. From the temperature profiles, it is found that cold temperatures (at 5 bars and 40 % cold mass fraction) of bend VT, converging VT and diverging VT are 276 K, 278 K, and 274 K respectively. In other words, at constant inlet pressure and cold mass fraction, the overall cold temperature of diverging VT is lower than bend VT followed by converging

VT. This shows that the thermal performance of diverging VT is better among these models.

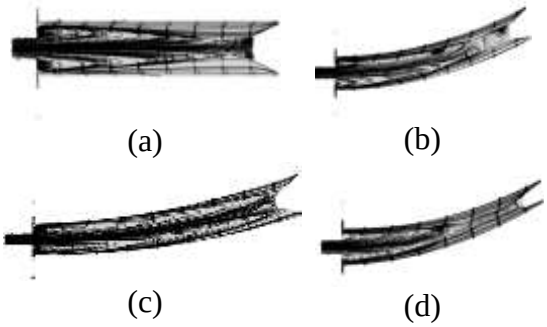

Figure 10 Veocity streamlines for: (a) Straight VT (b) Bend VT (c) Diverging VT (d) Converging VT

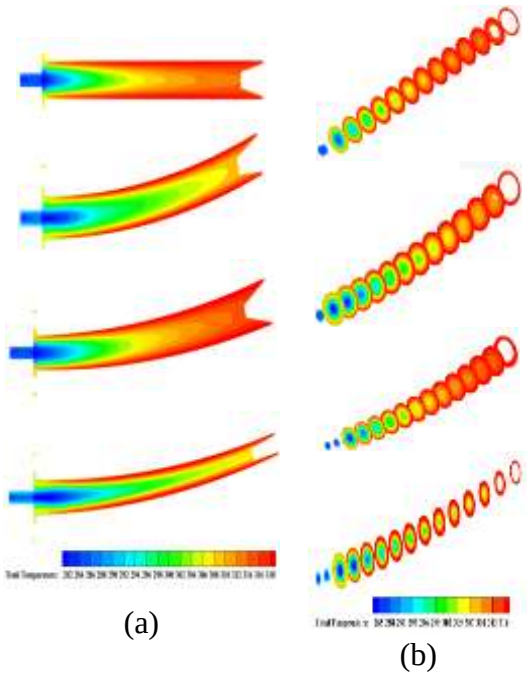

Figure 11 Total Temperature distribution: (a) YZ Plan cross-sections for each model (b) XY Plan cross-sections equally spaced for each model

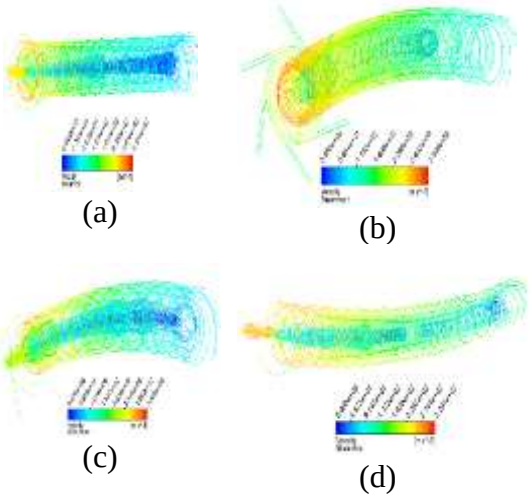

Figure 12 Swirl flow with velocity streamlines in (a) Straight VT (b) Bend VT (c) Diverging VT (d) Converging VT

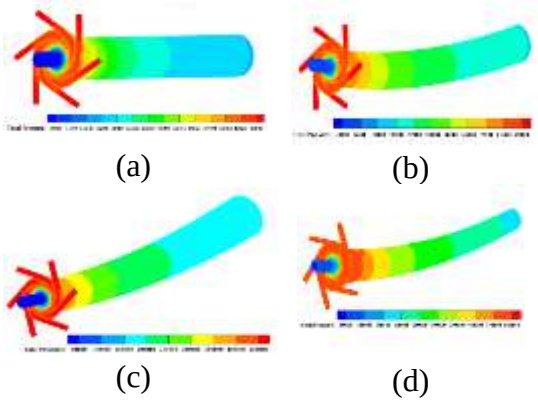

Figure 13 Pressure distribution in (a) Straight VT (b) Bend VT (c) Diverging VT (d) Converging VT

The flow visualizations are shown in different flow field diagrams. Figure 10 shows different velocity streamlines representing particles flow paths in two-dimensional slices. Secondary vortices can be seen between central and peripheral in these models which validates the theory of the secondary circulation as the cause of heat transfer from core flow to peripheral flow [12]. Although these secondary eddies are more dominantly found when the analysis is carried out in transient flow simulations.

To confirm the effectiveness and stability of cold temperature at the core region, different cross-sections are obtained as shown in Figure 11. The contours indicate that cold temperature flow is limited at the hot side in straight VT and diverging VT. However, in bend VT and converging VT, the cold flow almost reaches the frustum valve. To observe this effect more explicitly, equally spaced slices are extracted for temperature distribution in each model. It is cleared that the number of slices with cold temperature occurrence is mostly present in converging VT and bend VT. This indicates that converging VT has an undesirable effect of cooling potential on the hot side. Therefore, diverging VT can be preferred for its better cooling stability which mostly occurs near the cold orifice of the vortex tube.

One of the approaches to understanding the reasons behind the difference in thermal separation of these models is to study their velocity and pressure profiles. Figure 12 provides the three-dimensional swirl flow velocity profiles in which the maximum velocities noted for straight VT, bend VT, diverging VT, and converging VT are 333 m/s, 340 m/s, 356 m/s, and 320 m/s. Among these results, the highest velocity is attained by diverging VT whereas the lowest velocity is achieved by converging VT. One of the reasons for higher velocity in diverging VT is because of the broad conical working tube that encourages the particles to swirl with higher velocity as compared to converging VT where the working tube is narrower and therefore limits the particle velocity. Additionally, this effect can be described in terms of pressure contours since the pressure

distribution in converging VT working tube has higher among other models as shown in Figure 13. Since the swirl flow is turbulence dominating, therefore, the energetics of vortex tube flow is associated with turbulence properties. To link the turbulent flow with thermal separation phenomena, turbulent viscosity has been chosen as a turbulent property. A turbulent viscosity is one of the turbulent properties which identifies the degree of turbulences, greater the turbulent viscosity means more turbulence exists in the flow. Figure 14, shows the turbulent viscosity contours for each model in which the turbulent viscosity found maximum in diverging VT and minimum in converging VT. In other words, the maximum turbulence is found in diverging VT. Therefore, the presence of more turbulence yields improvement in thermal separation. This result is also in good agreement with the previous numerical studies [37].

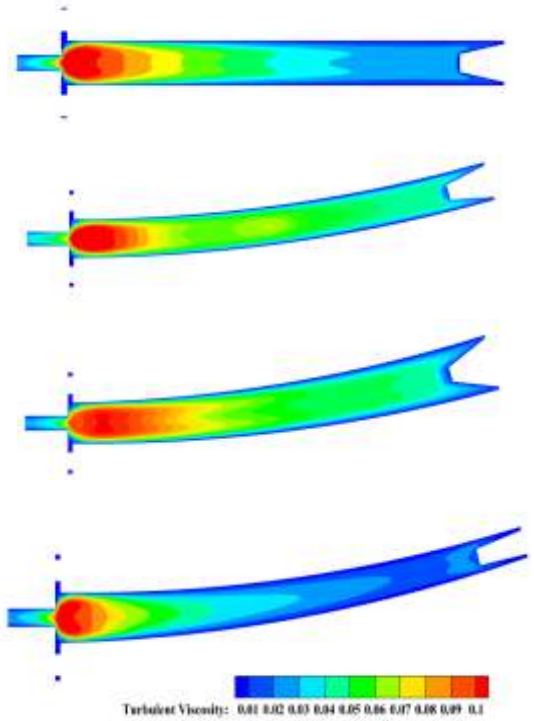

Figure 14 Turbulent viscosity distribution in each model

Coefficient of Performance Analysis of Vortex Tube

It is necessary to study the Coefficient of Performance (COP) of cooling for the given models. The relation for COP of refrigeration based on thermodynamic analysis is given by [38].

$$COP_R = \frac{\dot{Q}_L}{\dot{W}} \tag{10}$$

For cooling mode, the COP can be defined as the ratio of the cooling load to the compression power.

Where,

$$\dot{Q}_L = \dot{m}_L C_P (T_0 - T_L) \tag{11}$$

And

$$\dot{W} = \dot{m}_0 R T_0 \ln\left(\frac{P_0}{P_{atm}}\right) \tag{12}$$

So finally,

$$COP_R = \alpha \frac{k}{k-1} \frac{(1-\theta_L)}{\ln(R_P)} \tag{13}$$

Where "α" is the cold mass fraction, "k" is the ratio of heat capacities, in this case, its value is 1.4. "θ_L" represents the ratio of cold end temperature to total inlet temperature, and "R_P" is the pressure ratio between inlet and atmospheric pressures, respectively.

The COP_R of vortex tube is the final indicator that will conclude the performance of all these models. For this purpose,

COP_R of straight VT, bend VT, diverging VT, and converging VT are compared at 5 bars pressures. The pressure at the hot outlet is varied to vary the mass flow rate at the cold outlet. The COP_R has been calculated using Eqn. (13) for all these models. From Figure 15, it can be seen that COP_R of these models increases as the cold mass fraction increases. Since the cold mass fraction has a direct relation with the temperature elevation at the cold side. Therefore, there is exist an inverse relationship between the coldness effect at cold outlet and COP_R when varying cold mass fractions.

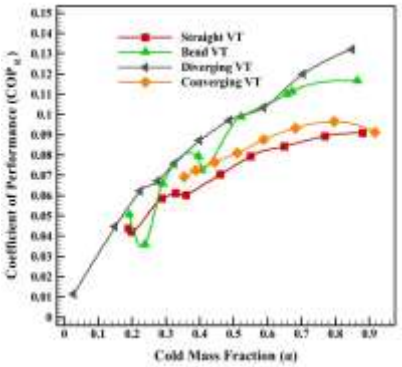

Figure 15 Effect of the cold mass fraction on COP_R for each model

From the results, it is found that COP_R of diverging VT is high throughout the cold mass fraction as compared to straight VT, bend VT, and converging VT. On the other hand, the COP_R of the bend VT tube fluctuates when the cold mass fraction increases.

Similarly, the $COP_R$of the converging VT is lower than that of diverging VT. This analysis shows that COP_R of vortex tube can be increased by incorporating a diverging bend working tube as a hot side of the vortex tube.

For quantitative measurement, it is necessary to find out the percentage increase in COP_R for the vortex tube, given as:

$$\%COP_R = \frac{COP_{Diverging\ VT} - COP_{Straight\ VT}}{COP_{Diverging\ VT}} \tag{14}$$

At 45% cold mass fraction, we have

$$\%COP_R = \frac{0.095 - 0.068}{0.068} = 0.397 \approx 40\% \quad (15)$$

Thus, from eqn. (15), it is found that the coefficient of performance of the vortex is improved by 40%.

V. CONCLUSION

In this study 3D, CFD steady-state simulations have been carried out to investigate the effect of different working tubes on the performance of vortex tube. For this purpose, a standard model of vortex tube is experimentally tested, and the results indicate that cold temperature drops as the cold mass fraction decreases. To perform 3D CFD simulations, a standard model vortex has been meshed in ICEM-CFD. Air is considered as fluid flow domain. The CFD model is then validated against experimental data in terms of the cold temperature of the vortex tube. the turbulence modeling is performed by using the standard k-ε model. Three extra models are then generated with specified working tubes as 16 degrees bend VT, 1 degree diverging, and converging vortex tube respectively. The simulations are performed in Fluent Ansys. Based on thermal separation and coefficient of performance, these models are compared, and the results indicate that diverging vortex tube has better performance among these models due to its diverging geometry that encourages more pressure expansion in a vortex tube. The percent increase in COP_R of modified vortex tube is almost increase by 40% as compared to standard model vortex tube.

NOMENCLATURE

VT	Vortex Tube	ρ	Density [kg/m^3]
P	Pressure [Pa]	K	Thermal
E	Total energy	T	conductivity[W/m
P_r	[Pa]	C_P	K]
μ	Prandtl number		Static temperature
μ_t	[---]	R	[K]
δ_{ij}	Dynamic	T_{IJ}	Specific heat at
z	viscosity	u_i	constant pressure
	[kg/ms]		[J/kgK]
	Turbulent	x_i	Gas constant
	viscosity		[J/kgK]
	[kg/ms]		Stress tensor
	Kronecker delta		component [---]
	[---]		velocity
	Axial distance		components i = 1,
	of working tube		2, 3 [m/s]
	[m]		coordinates i = 1,
			2, 3 [m]

REFERENCES

[1] Agarwal, G., McConkey Z. P., Hassard J., Optimisation of vortex tubes and the potential for use in atmospheric separation, J. Phys. D. Appl. Phys., 54, 2021, 9.

[2] Tsvetkov, O. B., Laptev, Y. A., Refrigerants and environment, J. Phys. Conf. Ser., 891, 2017.

[3] Jejurkar, A., Shukla, A. N., AN OVERVIEW ON VORTEX TUBE APPLICATIONS, Int. J. Adv. Eng. Res. Dev., 3, 2015.

[4] Kim, Y., Im, S., Han, J., A study on the application possibility of the vehicle air conditioning system using vortex tube, Energies, 13, 2020.

[5] Kim, Y., Im, S., Han, J., Air Conditioning System Using Vortex Tube, Energies, 13, 2020.

[6] Ranque, G. j., Method and apparatus for obtaining from a fluid under pressure two currents of fluid at different temperatures, 1934.

[7] Hilsch, R. The use of the expansion of gases in a centrifugal field as cooling process,Rev. Sci. Instrum., 18, 1947, 108–113.

[8] Kassner, R., Knoernschild, E., Friction laws and energy transfer in circular flow - Technical report no. F-TS-2198-ND, 1948.

[9] Fulton, C. D., Ranque's tube. J ASRE Refrigerating Eng., 58, 1950, 473–479.

[10] Kurosaka, M., Acoustic streaming in swirling flow and the Ranque-Hilsch (vortex-tube) effect, J. Fluid Mech., 124, 1982, 139–172.

[11] Stephan, K., Lin, S., Durst, M., Huang, F., Seher, D., An investigation of energy separation in a vortex tube, Int. J. Heat Mass Transf., 26, 1983, 341–348.

[12] Ahlborn, B., Groves, S., Secondary flow in a vortex tube, Fluid Dyn. Res., 21, 1997, 73–86.

[13] Fröhlingsdorf, W., Unger, H., Numerical investigations of the compressible flow and the energy separation in the Ranque-Hilsch vortex tube, Int. J. Heat Mass Transf., 42, 1998, 415–422.

[14] Nellis, G. F., Klein, S. A., The Application Of Vortex Tubes to Refrigeration Cycles (2002), International Refrigeration and Air Conditioning Conference. Paper 537.

[15] Kazantseva, O. V., Piralishvili, S. A., Fuzeeva, A. A., Numerical simulation of swirling flows in vortex tubes, High Temp., 43, 2005, 608–613.

[16] Skye, H. M., Nellis, G. F., Klein, S. A., Comparison of CFD analysis to empirical data in a commercial vortex tube, Int. J. Refrig., 2006,

[17] Sohn, C. H., Kim, C. S., Jung, U. H., Lakshmana Gowda B. H. L., Experimental and numerical studies in a vortex tube, J. Mech. Sci. Technol., 20, 2006, 418–425.

[18] Eiamsa-ard, S., Promvonge, P., Numerical investigation of the thermal separation in a Ranque-Hilsch vortex tube, Int. J. Heat Mass Transf., 50, 2007, 821–832.

[19] Rattanongphisat, W., Riffat, B., Gan, G., Thermal separation flow characteristic in a vortex tube: CFD model, Int. J. Low-Carbon Technol., 3, 2008, 282–295.

[20] Farouk, T., Farouk, B., Gutsol, A., Simulation of gas species and temperature separation in the counter-flow Ranque-Hilsch vortex tube using the large eddy simulation technique, Int. J. Heat Mass Transf., 52, 2009, 3320–3333.

[21] Baghdad, M., Ouadha, A., Imine, O., Addad, Y., Numerical study of energy separation in a vortex tube with different RANS models, Int. J. Therm. Sci., 50, 2011, 2377–2385.

[22] Thakare, H. R., Parekh, A. D., CFD analysis of energy separation of vortex tube employing different gases, turbulence models and discretisation schemes, Int. J. Heat Mass Transf., 78, 2014, 360–370.

[23] Bej, N., Sinhamahapatra, N. P., CFD study on the effects of viscous shear in a hot cascade Ranque-Hilsch vortex tube, IOP Conf. Ser. Mater. Sci. Eng., 101, 2015.

[24] Niknam, P., Mortaheb H. R., Mokhtarani B., Numerical Investigation of a Ranque–Hilsch Vortex Tube using a Three-Equation Turbulence Model, Chemical Engineering Communications, 204:3, 2017, 327-336.

[25] Nikitin, V., Bogdevičius, P., Bogdevičius, M., Overview of numerical methods for simulating Ranque-Hilsch effect within vortex tubes, 2015.

[26] Guo, X., Zhang, B., Computational investigation of precessing vortex breakdown and energy separation in a Ranque–Hilsch vortex tube, Int. J. Refrig., 85, 2018, 42–57, 2018.

[27] Chýlek, R., Šnajdárek, L., Pospíšil, J.,Vortex Tube: A Comparison of Experimental and CFD Analysis Featuring Different RANS Models, MATEC Web Conf., 168, 2018, 1–12.

[28] Guo, X., Zhang, B., Liu, B., Xu, X., A critical review on the flow structure studies of Ranque–Hilsch vortex tubes, Int. J. Refrig., 104, 2019, 51–64.

[29] Aljuwayhel, N. F., Nellis, G. F., Klein, S. A., Parametric and internal study of the vortex tube using a CFD model, International Journal of Refrigeration, 28, 2005, 442–450.

[30] Behera, U., Paul, P.J., Kasthurirengan, S., Karunanithi, R., Ram, S.N., Dinesh, K., Jacob, S., CFD analysis and experimental investigations towards optimizing the parameters of Ranque-Hilsch vortex tube, Int. J. Heat Mass Transf., 48, 2005, 1961–1973.

[31] Bramo A. R., Pourmahmoud, N., Computational fluid dynamics simulation of length to diameter ratio effects on the energy separation in a vortex tube, Therm. Sci., 15, 2011, 833–848.

[32] Pourmahmoud, N., Feyzi, A., Orang, A. A., Paykani, A., A parametric study on the performance of a Ranque-Hilsch vortex tube using a CFD-based approach, Mech. Ind., 16, 2015.

[33] Rafiee, S. E., Ayenehpour, S., Sadeghiazad, M. M., A study on the optimization of the angle of curvature for a Ranque–Hilsch vortex tube, using both experimental and full Reynolds stress turbulence numerical modelling, Heat Mass Transf. und Stoffuebertragung, 52, 2016, 337–350.

[34] Kandil H. A., Abdelghany, S. T., Computational investigation of different effects on the performance of the Ranque-Hilsch vortex tube, Energy, 84, 2015, 207–218.

[35] Bazgir, A., Nabhani, N., Bazooyar, B., Heydari, A., Computational Fluid Dynamic Prediction and Physical Mechanisms Consideration of Thermal Separation and Heat Transfer Processes Inside Divergent, Straight, and Convergent Ranque–Hilsch Vortex Tubes, J. Heat Transfer, 141, 2019.

[36] Shamsoddini R., Abolpour, B., A geometric model for a vortex tube based on numerical analysis to reduce the effect of nozzle number, Int. J. Refrig., 94, 2018, 49–58.

[37] Dutta, T., Sinhamahapatra, K. P., Bandyopdhyay, S. S., Comparison of different turbulence models in predicting the temperature separation in a Ranque-Hilsch vortex tube, Int. J. Refrig., 33, 2010, 783–792.

[38] Simões-Moreira, J. R. An air-standard cycle and a thermodynamic perspective on operational limits of Ranque-Hilsh or vortex tubes, Int. J. Refrig., 33,2010, 765–773.

AUTHORS

First Author – Fawad Ali, Faculty of Sciences, Aix-Marseille University, Jardin du Pharo, 58 Boulevard Charles Livon, Marseille, 13007, France.

Second Author – Muhammad Ali Kamran, PhD, Department of Mechanical Engineering, University of Engineering and Technology Peshawar, Pakistan.

Third Author – Mehran Meer, Tecnical Faculty, Friedrich-Alexander-Universität Erlangen-Nürnberg, Erwin-Rommel-Straße 60, Erlangen, 91058, Germany.

Fourth Author – Muhammad Hamza Awan, PhD, Department of Mechanical Engineering, University of Engineering and Technology Peshawar, Pakistan.

Fifth Author – Ameer Hamza, Department of Mechanical Engineering, University of Engineering and Technology Peshawar, Pakistan.

Sixth Author – Muhammad Alam Zaib Khan, PhD, Department of Mechanical Engineering, University of Engineering and Technology Peshawar, Pakistan.

Correspondence Author – Muhammad Alam Zaib Khan, PhD, Department of Mechanical Engineering, University of Engineering and Technology Peshawar, Pakistan.